Hydrodynamic performances of wave energy converter arrays in front of a vertical wall

KARA, Fuat

Hydrodynamic performances of wave energy converter arrays in front of a vertical wall

Fuat Kara, Sheffield Hallam University, Howard Street, Sheffield, S1 1WB, UK, fuat.kara@shu.ac.uk

Abstract

Wave power absorption with Wave Energy Converters (WECs) arrays in front of a vertical wall is predicted with an in-house transient wave-multibody numerical tool of ITU-WAVE which uses time marching scheme to solve a boundary integral equation for the analyses of hydrodynamic radiation and exciting forces. The perfect reflection of incident waves from a vertical wall is considered with method of images. Mean interaction factor, which can have constructive or destructive effect and determines the performances of WECs, is approximated with different array configurations. The vertical wall effect plays significant role over hydrodynamic parameters as the radiation and exciting forces show quite different behaviour in the case of WECs with and without vertical wall in an array system. The numerical results show that the performance and wave power absorption with WECs arrays in front of vertical wall are much greater compared to WECs arrays without vertical wall effect. This is mainly due to standing and nearly trapped waves between a vertical wall and WECs arrays in addition to strong interactions between WECs. The satisfactory agreements are obtained when the present ITU-WAVE numerical results for different hydrodynamic parameters in an array system are compared with other published analytical and numerical results.

Keywords: method of images; wave power absorption with arrays; mean interaction factor; transient wave Green function; multibody interaction in front of a vertical wall; boundary integral equation

1. Introduction

Wave energy from ocean waves can be absorbed with or without a coastal structures effect (e.g., a vertical wall) using isolated, linear, square, or rectangular WECs arrays. The efficiency of these options depends on the geometries of WECs and WECs array configurations, control strategies to maximise the absorb wave power (Kara 2010), Power-Take-Off (PTO) systems, incoming wave heading angles (Kara 2016a), single mode of motion (e.g., heave or pitch) or multimode (e.g., heave and pitch). In addition to these parameters, in the case of WECs arrays in front of a vertical wall, the efficiency also depends on the separation distance between WECs (Kara 2016a) as well as a vertical wall and WECs. Although the installations, operations, and maintenances of WECs arrays at the offshore environment increase the overall cost significantly, the overall cost can be reduced by integrating WECs arrays with other coastal structures or placing WECs in front of coastal structures. As expected, the significant amount of wave power can be absorbed with WECs arrays compared to isolated WEC. This is mainly due to the hydrodynamic interactions between a vertical wall and WECs arrays as well as nearly trapped waves in the gap of array configurations (Mustapa et.al., 2017; Zhao et.al., 2019a).

The high energy costs can also be reduced by optimising the geometry of WECs (to increase hydrodynamic performances), control strategies (to improve efficiencies), and mechanical components (to avoid energy loses). In addition, using already available grid systems would result in to avoid additional cost and environmental impact effects. When the performance of WECs arrays in front of a vertical wall is compared with those of integration of WECs arrays with other maritime structures, it is found out that previous one shows the superiority although the deployments of mooring systems, installations, and maintenances are more challenging for WECs placed in front of a vertical wall (Mustapa et.al., 2017). This is mainly due to the improved efficiency of WECs arrays resulting from the optimised hydrodynamic interactions with the reflected waves from a vertical wall and WECs in an array system.

The behaviour and performance of WECs in front of a vertical wall are studied both experimentally and numerically to define the effect of hydrodynamic interactions between a vertical wall and WECs arrays. The separation distances between a vertical wall and WECs as well as between WECs arrays play significant role on the maximum wave power absorption and performance of the array systems due to vertical wall effects (Schay et.al., 2013). The wave interaction and nearly trapped waves in the gap of WECs as well as a vertical wall and WECs can be used to increase the competitiveness and enhance the efficiency of array system. The performances of WEC arrays are studied with options of integrating or placing them in front of other maritime structures using different configurations including stationary and floating systems (e.g., Oscillating Water Column, Overtopping, oscillating buoys) (Michele et.al., 2019; Buriani et.al., 2017, Michele et.al., 2016; Ning et.al., 2016; Contestabile et.al., 2016; Sarkar et.al., 2015; He et.al., 2013).

Impulse Response Functions (IRFs) of WECs arrays in front of a vertical wall, which is considered as the symmetry lines, can be predicted with method of images to approximate the flow behaviour around WECs arrays. The isolated WEC or WECs in an array system and their images with this method are used for the prediction of the frequency dependent radiation added-mass and damping coefficients as well as exciting forces in a channel or in front of vertical wall (Newman, 2016; Zhao et.al., 2019b). Method of images considers the vertical wall as infinite wall (Konispoliatis et.al., 2020) assuming infinite length and perfect reflection of incident waves. Alternatively, the vertical wall can be also considered as a finite wall (Loukogeorgaki et.al., 2020) considering the effect of finite length of the vertical wall on the hydrodynamic performances of WECs in an array system.

Analytical and numerical methods in two and three dimensions are used for the prediction of the wave power absorption in front of a vertical wall which is the function of exciting and radiation forces. The frequency domain methods in two (McIver and Porter, 2016) or three dimensions (Zheng and Zhang, 2016; Schay et.al., 2013) as well as time domain methods with three-dimensional wave Green function can be used to predict the wave power absorption in front of a vertical wall. The strips in strip theory are used in two-dimensional methods in which the interaction effects between the strips are not considered. This limitation of two-dimensional methods can be removed using three dimensional methods as the interactions between discretised panels are taken automatically into account. As two and three-dimensional frequency domain methods are inherently linear, nonlinear effect can only be considered with two- or three-dimensional time domain methods which are used in the present study.

There are three commonly used three-dimensional methods in both frequency and time domain to predict the hydrodynamic exciting and radiation forces of WECs in front of a vertical wall. These three-dimensional methods take the hydrodynamic interactions between WECs and a vertical wall as well as between WECs into account. Rankine panel (Nakos et.al., 1993; Kring and Sclavounos, 1995) and wave Green function methods in both frequency and time domains (Chang, 1977; Kara, 2020, 2016a, 2016b) are the most used Boundary Integral Equations Methods (BIEM) which are the numerical methods used to predict the hydrodynamic parameters of floating systems. As wave Green function satisfies the condition at infinity and free-surface boundary conditions automatically, hydrodynamic parameters are predicted by discretising the body surface only to satisfy the body boundary condition. However, in the case of Rankine panel methods, body boundary condition, condition at infinity and free-surface boundary conditions are satisfied numerically by discretising both some part of free surface and body surface which increase the computational time considerably. The third types of the methods are the analytical methods at which WEC geometries (e.g., sphere, vertical cylinder) are defined analytically. The analytical methods include direct matrix method (Kagemoto and Yue, 1986), plane wave analysis (Ohkusu, 1972) and point absorber (Budal, 1977). The direct matrix method is extensively used in academia and industry due to its accurate predictions of the hydrodynamic performances of floating bodies in an array system.

The wave energy absorption from ocean waves with WEC arrays in front of a vertical wall did not get much attention in the open literature compared to the exploitation of WECs without vertical wall effect. The efficiency of WECs arrays can be increased using a vertical wall which magnifies the absorbed wave power. In the context of hydrodynamic performance of WECs in front of a vertical wall, most of the papers in the literature is focused on the exciting forces due to incident and diffracted waves whilst the hydrodynamic radiation forces due to oscillations of WECs in an array system did not get much attention. The shortcoming of the existence literature in these fields will be filled with the present work. In addition, to the best of the authors' knowledge, the free-surface transient wave Green function is not used before for the prediction of the hydrodynamic radiation and exciting force parameters of WECs arrays in front of a vertical wall. This is an additional novel contribution to the knowledge in this field by the present study.

Method of images assuming infinite vertical wall length is used in the present paper to predict the time dependent diagonal and interaction IRFs of exciting forces, which are the superposition of diffraction and Froude-Krylow forces, and radiation forces for 1x5, 2x5, 3x5, 4x5 and 5x5 sphere WECs arrays in front of a vertical wall at sway and heave modes. Fourier transform of IRFs is then used to obtain the frequency dependent exciting force amplitude as well as radiation added-mass and damping coefficients. These frequency dependent hydrodynamic parameters are then compared with other published numerical and analytical results for the validation of the present three-dimensional ITU-WAVE numerical results. The absorbed wave power, which are the functions of the hydrodynamic exciting and radiation forces, is directly predicted in time domain taking the average of instantaneous wave power signals. The contribution of transient effects on numerical results for wave power prediction is avoided by using only last half of the instantaneous wave power signals.

2. Numerical modelling of WECs arrays in front of a vertical wall

2.1. Equation of motion of WECs in an array system

The right-handed body-fixed Cartesian coordinate system $\vec{x} = (x, y, z)$ for the solution of initial value problem is used to determine the fluid flow around WECs arrays in front of a vertical wall as presented in Figure 1. The coordinate system is placed on the free-surface and coincides with z=0 or xy-plane whilst the origin of the coordinate system is on the middle of the vertical wall. The positive z- and x-directions are towards upward and forward respectively. WECs arrays in front of a vertical wall oscillates at their mean position due to impulsively exited incident waves at the origin of the body fixed coordinate system. The boundaries of the initial-value problem are presented with surface at infinity S_∞ in Figure 1. Furthermore, the free surface is given with $S_f(t)$ whilst the surface at intersection between body and free surface is presented with $\Gamma(\mathrm{t})$. In addition, body surface is given with $S_b(t)$ whilst the surface of a vertical wall is presented with $S_{wl}(t)$ in Figure 1 (Kara, 2020).

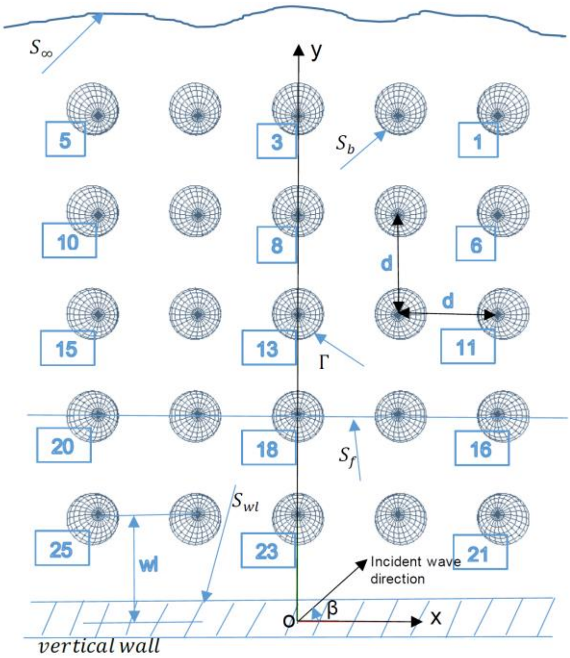

Figure 1: Coordinate system and surfaces of 5x5 WECs arrays of sphere in front of a vertical wall in xy-plane

In Figure 1, the position of WECs in front of a vertical wall is given with numbers (1, 2, 3,…,25). The incident wave heading angles are presented with β and $\beta = 90°$ is used for beam seas whilst $\beta = 180°$ is used for head seas. d is the separation distance between WECs whilst wl is the separation distance between last row of WECs (e.g., WEC21, …, WEC25) and the vertical wall in Figure 1.

The hydrodynamic performances of WECs arrays in time domain are solved assuming that fluid is inviscid and incompressible, and its flow is irrotational such that there are no lifting effects and fluid separation. These assumptions on fluid and its flow result in using the potential theory and implicitly also mean that the time dependent flow velocity $\vec{V}(\vec{x}, t)$ can be represented as the gradient of the velocity potential $\vec{V}(\vec{x}, t) = \nabla\Phi(\vec{x}, t)$. The use of potential theory also means that Laplace equation $\nabla^2\Phi(\vec{x}, t) = 0$ dictates the solutions of the time dependent velocity potentials $\Phi(\vec{x}, t)$.

The time dependent equation of motion of WECs arrays in front of a vertical wall in Eq. (1) is the functions of acceleration relevant to inertia terms, hydrostatic restoring forces, and time dependent hydrodynamic restoring forces and exciting force parameters (Cummins 1962). The effects of the incident waves result in the pressure changes around WECs arrays which cause the oscillations of WECs. The oscillating WECs in an array system generate the radiated waves on the free surface which are presented by the convolution integral on the left-hand side of Eq. (1) whilst the effects of incident and diffracted waves are presented with convolution integral on the right-hand side of Eq. (1).

$$\sum_{k=1}^{6}\left(M_{kk_i}+a_{kk_i}\right)\ddot{x}_{k_i}(t)+\left(b_{kk_i}+B_{PTO-kk_i}\right)\dot{x}_{k_i}(t)+\left(C_{kk_i}+c_{kk_i}+C_{PTO-kk_i}\right)x_{k_i}(t)+\int_0^t d\tau K_{kk_i}(t-\tau)\dot{x}_{k_i}(\tau)$$

$$=\int_{-\infty}^{\infty} d\tau K_{kD_i}(t-\tau)\zeta(\tau) \quad (1)$$

where upper boundary of sum $k = 1, 2, 3, \ldots, 6$ represents the rigid modes of motions of surge, sway, heave, roll, pitch, and yaw respectively whilst index $i = 1, 2, 3, \ldots, N$ is for number of WECs in an array system. $x_k(t) = (1, 2, 3, \ldots, N)^T$, $\dot{x}_k(t)$ and $\ddot{x}_k(t)$, where dots represent time derivatives, is used for displacements, velocities, and accelerations, respectively. M_{kk} is the inertia mass matrix whilst C_{kk} is the hydrostatic restoring coefficients in Eq. (2). m and C are the inertia mass and restoring coefficient of an isolated WEC respectively. As the same radius R is used for all spheres in WECs arrays, the restoring force and inertia mass of each WEC are the same $C_1 = C_2 = \cdots = C_N = C$ and $m_1 = m_2 = \cdots = m_N = m$ respectively.

$$M_{kk}=\begin{pmatrix} m_1 & \cdots & 0 \\ \vdots & \ddots & \vdots \\ 0 & \cdots & m_N \end{pmatrix},\ C_{kk}=\begin{pmatrix} C_1 & \cdots & 0 \\ \vdots & \ddots & \vdots \\ 0 & \cdots & C_N \end{pmatrix} \ (2)$$

The time and frequency independent restoring coefficient c_{kk}, damping coefficient b_{kk} and infinite added mass a_{kk} coefficients in Eq. (3) depend on geometry and are relevant to displacement, velocity, and acceleration, respectively. The interaction terms are represented with off-diagonal terms whilst the diagonal terms represent the contribution of each WEC in an array system. IRF $K_{kk}(t)$, which is the function of the time and geometry, represent the force on k-th body due to the impulsive velocity of k-th body. The oscillations of WECs in an array system cause the disturbance of free surface which is known as the memory effect of the fluid responses. The convolution integral on the left-hand side of Eq. (1) are used to represent the memory effect and the effect of the wave damping (Ogilvie 1964).

$$K_{kk}(t)=\begin{pmatrix} K_{11} & \cdots & K_{1N} \\ \vdots & \ddots & \vdots \\ K_{N1} & \cdots & K_{NN} \end{pmatrix}, a_{kk}=\begin{pmatrix} a_{11} & \cdots & a_{1N} \\ \vdots & \ddots & \vdots \\ a_{N1} & \cdots & a_{NN} \end{pmatrix}, b_{kk}=\begin{pmatrix} b_{11} & \cdots & b_{1N} \\ \vdots & \ddots & \vdots \\ b_{N1} & \cdots & b_{NN} \end{pmatrix}, c_{kk}=\begin{pmatrix} c_{11} & \cdots & c_{1N} \\ \vdots & \ddots & \vdots \\ c_{N1} & \cdots & c_{NN} \end{pmatrix} \ (3)$$

The origin of the body-fixed coordinate system in Figure 1 is used to predict the time dependent exciting force IRFs $K_{kE}(t) = (K_{1E}, K_{2E}, K_{3E}, \ldots, K_{NE})^T$ on the k-th body due to impulsive incident wave elevation $\zeta(t)$, which is a uni-directional incoming wave system with arbitrary heading angles, as presented in Eq. (4). The superposition of diffraction and Froude-Krylov IRFs results in the exciting forces and moments $K_{kE}(t)$ in time on the right-hand side of Eq. (1) (King, 1987).

$$F_{kE}(t)=\int_{-\infty}^{\infty} d\tau K_{kE_i}(t-\tau)\zeta(\tau) \qquad (4)$$

The elements of PTO in Eq. (5) are the time independent and frequency dependent wave damping coefficient B_{PTO-kk} matrix and C_{PTO-kk} which is the time and frequency independent restoring coefficient matrix. It is theoretically known that the maximum wave power is absorbed at the resonant frequency (Budal and Falnes, 1976). It is the reason that the diagonal elements of PTO matrix B_{PTO-kk} in Eq. (5) are selected as the wave damping at the resonant frequency at which the natural frequency of isolated WEC and incident wave excitation frequency are equal. For the simplicity purpose, the off-diagonal terms of PTO matrix, which represent the wave damping due to cross-interaction between WECs in an array system, are considered zero. The elements of C_{PTO-kk} are considered zero for heave mode while for sway mode, the diagonal elements of C_{PTO-kk} are taken the same as hydrostatic restoring coefficient of heave mode to have the same natural frequency and displacement in both heave and sway modes. In this case, it would be possible to compare heave and sway motions and power variables directly to decide which modes of motion are more effective and efficient for power absorption.

$$B_{PTO-kk} = \begin{pmatrix} B_{iso}(\omega_n) & \cdots & 0 \\ \vdots & \ddots & \vdots \\ 0 & \cdots & B_{iso}(\omega_n) \end{pmatrix}, \; C_{PTO-kk} = \begin{pmatrix} C_1 & \cdots & 0 \\ \vdots & \ddots & \vdots \\ 0 & \cdots & C_N \end{pmatrix} \quad (5)$$

where the natural frequency of each isolated WEC is given with ω_n. The time marching scheme with fourth order Runge-Kutta method (Kara 2016b, 2015) can be used to solve the equation of motion Eq. (1) after determination of PTO damping B_{PTO-kk}, restoring C_{PTO-kk} matrices, and inertia mass matrix M_{kk}. The time and frequency independent added-mass at infinite wave frequency a_{kk}, wave damping b_{kk} and restoring c_{kk} coefficients are also input for Eq. (1). In addition, Eq. (1) at each time step requires the hydrodynamic restoring or wave damping which is represented with convolution integral on the left-hand side of Eq. (1) and is the function of the radiation IRFs and velocity of WECs. Furthermore, the exciting force at each time step is also required and represented with convolution integral on the right-hand side of Eq. (1).

2.2. Integral equation of WECs in an array system

The transient wave Green function is used to solve the initial value problem which can be modelled as a surface integral equation and requires the satisfaction of the initial condition, free surface boundary condition, body boundary condition and condition at infinity. The transient wave Green function satisfy the free-surface boundary condition and condition at infinity automatically which means only body boundary condition need to be satisfied numerically (Wehausen and Laitone 1960). The transient boundary integral equation of the source strength in time on WECs in an array system (Kara 2020) is obtained by applying Green's theorem and using the properties of the transient wave Green function and potential theory in Eq. (6).

$$\begin{cases} \sigma_1(\mathrm{P,t}) + \dfrac{1}{2\pi}\iint_{S_1} \mathrm{dS_Q}\dfrac{\partial}{\partial \mathrm{n_P}}\mathrm{G(P,Q,t-\tau)}|_{S_1}\sigma_1(\mathrm{Q,t}) + \cdots + \dfrac{1}{2\pi}\iint_{S_N} \mathrm{dS_Q}\dfrac{\partial}{\partial \mathrm{n_P}}\mathrm{G(P,Q,t-\tau)}|_{S_1}\sigma_N(\mathrm{Q,t}) = -2\dfrac{\partial}{\partial \mathrm{n_P}}\phi(\mathrm{P,t})|_{S_1} \\ \vdots \\ \sigma_N(\mathrm{P,t}) + \dfrac{1}{2\pi}\iint_{S_1} \mathrm{dS_Q}\dfrac{\partial}{\partial \mathrm{n_P}}\mathrm{G(P,Q,t-\tau)}|_{S_N}\sigma_1(\mathrm{Q,t}) + \cdots + \dfrac{1}{2\pi}\iint_{S_N} \mathrm{dS_Q}\dfrac{\partial}{\partial \mathrm{n_P}}\mathrm{G(P,Q,t-\tau)}|_{S_N}\sigma_N(\mathrm{Q,t}) = -2\dfrac{\partial}{\partial \mathrm{n_P}}\phi(\mathrm{P,t})|_{S_N} \end{cases} \tag{6}$$

and the time dependent potential on each WEC in an array system

$$\begin{cases} \phi_1(\mathrm{P,t}) = -\dfrac{1}{4\pi}\iint_{S_1} \mathrm{dS_Q G(P,Q,t-\tau)}|_{S_1}\sigma_1(\mathrm{Q,t}) - \cdots - \dfrac{1}{4\pi}\iint_{S_N} \mathrm{dS_Q G(P,Q,t-\tau)}|_{S_1}\sigma_N(\mathrm{Q,t}) \\ \vdots \\ \phi_N(\mathrm{P,t}) = -\dfrac{1}{4\pi_1}\iint_{S_1} \mathrm{dS_Q G(P,Q,t-\tau)}|_{S_N}\sigma_1(\mathrm{Q,t}) - \cdots - \dfrac{1}{4\pi}\iint_{S_N} \mathrm{dS_Q G(P,Q,t-\tau)}|_{S_N}\sigma_N(\mathrm{Q,t}) \end{cases} \tag{7}$$

where the transient Green function, which has time dependent and time independent parts, is given by $\mathrm{G(P,Q,t-\tau)} = \left(\frac{1}{r} - \frac{1}{r'}\right)\delta(\mathrm{t-\tau}) + \mathrm{H(t-\tau)}\widetilde{\mathrm{G}}(\mathrm{P,Q,t-\tau})$ in which the time independent part is known as Rankine parts and are presented with $\left(\frac{1}{r} - \frac{1}{r'}\right)$ whilst the time dependent part is known as transient or memory part and is given by $\widetilde{\mathrm{G}}(\mathrm{P,Q,t-\tau})$ which represents the free surface effect due to oscillation of WECs in an array system. The interactions of the discretised surface panels are given with $\mathrm{r} = \sqrt{(\mathrm{x}-\xi)^2 + (\mathrm{y}-\eta)^2 + (\mathrm{z}-\zeta)^2}$ which represents the distance between field points $\mathrm{P(x,y,z)}$ and source or integration points $Q(\xi,\eta,\zeta)$ whilst the image part that is distance between field point and image integration point above free surface is presented with $\mathrm{r}' = \sqrt{(\mathrm{x}-\xi)^2 + (\mathrm{y}-\eta)^2 + (\mathrm{z}+\zeta)^2}$. Dirac delta function and Heaviside unit step function are presented with $\delta(\mathrm{t-\tau})$ and $\mathrm{H(t-\tau)}$ respectively. WECs in an array system are discretised with quadrilateral panels and analytical integrations (Hess and Smith 1964) are used to predict the solution of Rankine parts $\left(\frac{1}{r}, \frac{1}{r'}\right)$. The mixed solution methods for the surface integration are used depending on the distance between field points $\mathrm{P(x,y,z)}$ and integration points $Q(\xi,\eta,\zeta)$. The exact solution, a multi-pole extension and a monopole expansion are used for the small, intermediate, and large values of $\mathrm{r}(P,Q)$ respectively.

$\widetilde{\mathrm{G}}(\mathrm{P,Q,t-\tau}) = 2\int_0^\infty \mathrm{dk}\sqrt{\mathrm{kg}}\sin(\sqrt{\mathrm{kg}}(\mathrm{t-\tau}))e^{\mathrm{k(z+\zeta)}}\mathrm{J_0(kR)}$ represents the transient or memory part where $\mathrm{J_0(kR)}$ is the zero order Bessel function. k is the wave number whilst $R = \sqrt{(\mathrm{x}-\xi)^2 + (\mathrm{y}-\eta)^2}$ is the distance between field points $\mathrm{P(x,y,z)}$ and integration points $Q(\xi,\eta,\zeta)$ on the free surface. g is gravitational acceleration. The solution of transient wave part $\widetilde{\mathrm{G}}(\mathrm{P,Q,t-\tau})$ of Green function

$G(P, Q, t-\tau)$ over quadrilateral panels are mapped into a unit square and then are integrated numerically with 2x2 two-dimensional Gaussian quadrature after the solution of the transient wave Green function analytically $\widetilde{G}(P, Q, t-\tau)$ (Liapis 1986, King 1987, Kara 2000). The prediction of memory part $\widetilde{G}(P, Q, t-\tau)$ is the computationally expensive so that it is important to use accurate and efficient methods. As only one kind of analytical method cannot be used for the solution due to convergence problems, five analytical methods depending on time and space parameters, which are function of relative position of field and integration points, are used to predict the time dependent wave Green function $\widetilde{G}(P, Q, t-\tau)$ part including asymptotic expansion of complex error function, Bessel function, Filon quadrature, asymptotic expansion, and power series expansion.

The time dependent potentials $(\phi_1, \phi_2, \phi_3, \dots, \phi_N)$ in Eq. (7), N being the number of WECs in an array system, is predicted with time marching scheme after the solution of the time dependent boundary integral equations for source strengths $(\sigma_1, \sigma_2, \sigma_3, \dots, \sigma_N)$ in Eq. (6). The time dependent fluid velocities are then calculated as the gradient of the potentials $(\nabla\phi_1, \nabla\phi_2, \nabla\phi_3, \dots, \nabla\phi_N)$. The only difference for the solution of the boundary integral equation of the radiation and diffraction problems is the time dependent body boundary conditions, which are the terms on the right-hand-side of Eq. (6). Eq. (6) can be used for the predictions of both radiation and diffraction time dependent source strengths $(\sigma_1, \sigma_2, \sigma_3, \dots, \sigma_N)$, which describe the flow behaviour around WECs in an array system. As the condition at infinity and free-surface boundary condition are satisfied automatically by the transient wave Green Function part $\widetilde{G}(P, Q, t-\tau)$, only the body surfaces beneath free surface of WECs in an array system is discretised with quadrilateral elements over which the constant source strengths are used for the solution of the boundary integral equation Eq. (6) in time. The discretisation of the surfaces of WECs in an array system implies that unknown finite number of the source strengths $(\sigma_1, \sigma_2, \sigma_3, \dots, \sigma_N)$ are replaced with continuous singularity distributions. The collocation points of each quadrilateral elements are used to satisfy the boundary integral equation Eq. (6) which results in a system of algebraic equation for the prediction of the time dependent source strengths $(\sigma_1, \sigma_2, \sigma_3, \dots, \sigma_N)$ on each quadrilateral element.

2.3. Instantaneous and mean absorbed wave power

The instantaneous wave power $P_{ins_{k_i}}(t)$ from ocean waves is converted to useful electrical energy at each mode of motion from each WEC in an array system with PTO system. The time dependent instantaneous absorbed wave power $P_{ins_{k_i}}(t)$ is presented in Eq. (8) and is the functions of exciting force, radiation force, and velocity of each WEC placed in front of a vertical wall.

$$P_{ins_{k_i}}(t) = [F_{exc_{k_i}}(t) + F_{rad_{k_i}}(t)] \cdot \dot{x}_{k_i}(t) \qquad (8)$$

where $F_{exc_{k_i}}(t)$ in Eq. (9) is the time dependent exciting force due to incident and diffracted waves and $F_{rad_{k_i}}(t)$ in Eq. (10) is the radiation force due to oscillation of each WEC in an array system whilst the velocities of each WEC in front of a vertical wall are presented with $\dot{x}_{k_i}(t)$ (Kara 2010, 2016a).

$$F_{exc_{k_i}}(t) = F_{k_i}(t) = \int_{-\infty}^{\infty} d\tau K_{kD_i}(t-\tau)\zeta(\tau) \quad (9)$$

$$F_{rad_{k_i}}(t) = F_{kk_i}(t) = -a_{kk_i}\ddot{x}_{k_i}(t) - b_{kk_i}\dot{x}_{k_i}(t) - c_{kk_i}x_{k_i}(t) - \int_0^t d\tau K_{kk_i}(t-\tau)\dot{x}_{k_i}(\tau) \qquad (10)$$

The product of time dependent exciting force $F_{exc_{k_i}}(t)$ in Eq. (9) and WEC velocity $\dot{x}_{k_i}(t)$ results in the absorbed total exciting wave power $P_{exc_{k_i}}(t) = F_{exc_{k_i}}(t) \cdot \dot{x}_{k_i}(t)$ from incident wave at any heading angles. The product of time dependent velocity $\dot{x}_{k_i}(t)$ and radiation force $F_{rad_{k_i}}(t)$ in Eq. (10) results in radiation wave power $P_{rad_{k_i}}(t) = F_{rad_{k_i}}(t) \cdot \dot{x}_{k_i}(t)$ which is the power that is radiated back to sea. The absorbed mean wave power $\bar{P}_{ins_{k_i}}(t)$ with PTO system from ocean waves over a range of time T in Eq. (11) is averaged to predict the absorbed useful wave power.

$$\bar{P}_{ins_{k_i}}(t) = \frac{1}{T}\int_0^T dt \cdot [F_{exc_{k_i}}(t) + F_{rad_{k_i}}(t)] \cdot \dot{x}_{k_i}(t) \quad (11)$$

where T is the total simulation time and Eq. (11) is approximated directly with numerical integration

$$\bar{P}_{ins_{k_i}}(t_j) \cong \frac{1}{n_j}\sum_{j=1}^{n_j}[F_{exc_{k_i}}(t_j) + F_{rad_{k_i}}(t_j)] \cdot \dot{x}_{k_i}(t_j) \quad (11a)$$

where $j = 1, 2, 3, \ldots, t_N$. t_N is the total number of time step whilst n_j is the number of samples ($T = n_j \Delta t$). Δt is the time step size. The transient effects are avoided considering only the last half of the simulation to predict the time dependent parameters including the averaged (mean) absorbed wave power in Eq. (11a).

$$\bar{P}_{T_k}(t) = \sum_{i=1}^{N} \bar{P}_{ins_{k_i}}(t) \qquad (12)$$

The time dependent absorbed total mean wave power $\bar{P}_{T_k}(t)$ in Eq. (12) at mode of motion of k is the superposition of the mean wave power that is absorbed with each $i-th$ WEC in an array system in front of a vertical wall with N numbers of WECs.

2.4. Mean interaction factor

The mean interaction factor $q_{mean,k}(\omega)$ at any incident wave frequency is used to measure the gain factor due to the interaction of WECs in an array system in front of a vertical wall. $q_{mean,k}(\omega)$ is the functions of wave power absorbed by N interacting WECs and an isolated WEC at any given heading angles. The constructive $(q_{mean,k}(\omega) > 1)$ and destructive $(q_{mean,k}(\omega) < 1)$ effects of mean interaction factor $q_{mean,k}(\omega)$ depend on the separation distance between WECs as well as a vertical wall and WECs, incident wave heading angles, geometry of WECs, and control strategies to improve the efficiency of WECs in an array system.

The frequency dependent mean interaction factor $q_{mean,k}(\omega)$ at any incident wave frequency in Eq. (13) is given as the ratio of the sum of mean absorbed wave power with N number of WECs in an array system in front of a vertical wall to N times the mean absorbed wave power with an isolated WEC at the resonant frequency (Thomas & Evans 1981).

$$q_{mean,k}(\omega) = \frac{\bar{P}_{T_k}(\omega)}{N \times \bar{P}_{ins_{k_0}}(\omega_n)} \quad (13)$$

where N is the number of WECs in an array system. The sum of the mean absorbed wave power at any mode of motion k is given with $\bar{P}_{T_k}(\omega)$ at any given incident wave frequency ω whilst the mean absorbed wave power with an isolated WEC is given with $\bar{P}_{ins_{k_0}}(\omega_n)$ at the resonant frequency ω_n. $\bar{P}_{T_k}(\omega)$ at the incident wave frequency ω is the mean value of $\bar{P}_{T_k}(t)$ in Eq. (12) whilst $\bar{P}_{ins_{k_0}}(\omega_n)$ at the natural frequency ω_n is the mean value of $\bar{P}_{ins_{k_0}}(t)$.

3. Numerical results and discussions of WECs in an array system

The present numerical results of hydrodynamic parameters (e.g., exciting and radiation IRFs, exciting force amplitudes, added-mass and damping coefficients) and wave power absorptions from ocean waves with WECs in an array system with and without a vertical wall effect are predicted with in-house transient wave-multibody interaction computational tool of ITU-WAVE (Kara, 2021, 2020, 2016a, 2016b, 2015, 2010, 2000).

3.1. Validation of ITU-WAVE numerical results with analytical and other numerical results

The present ITU-WAVE numerical results of diagonal and interaction added-mass and damping coefficients, exciting force amplitudes, and mean interaction factors of absorbed wave power are validated against different configurations of WECs arrays including 1x5 and 2x2 arrays of truncated vertical cylinder in front of a vertical wall and 2x5 arrays of vertical cylinder with hemisphere bottom without vertical wall effect.

3.1.1. Truncated vertical cylinder of 1x5 arrays in front of a vertical wall – radiation forces

The method of images in the present ITU-WAVE numerical tool is used to predict the hydrodynamic parameters of 1x5 linear arrays of truncated vertical cylinders. The analytical results of Konispoliatis et.al. (2020) is then used for the validation of ITU-WAVE numerical results. The convergence test is conducted in space and time which are converged with 256 panels for each WEC in space and 0.05 nondimensional time step size $\Delta t\sqrt{g/R}$ in time. When surge and sway mode nondimensional diagonal IRFs are compared in Figure 2(a), it can be observed that surge IRF decays faster at larger nondimensional time steps of 15 and 25. As the area under IRFs represents the energy to be captured (Kara, 2020, 2016a), this implicitly means that sway mode stores more energy at larger times compared to surge mode. The nondimensional interaction IRFs in sway mode between WEC1 and WEC2 (K_{12}) as well as between WEC1 and WEC3 (K_{13}) are shown in Figure 2(b). The behaviour of diagonal IRF in Figure 2(a) and interaction IRFs in Figure 2(b) in sway mode are quite different. The interaction IRFs show greater oscillation amplitudes at larger times whilst diagonal IRF decays to zero just after nondimensional time step of 4. It can be also seen in Figure 2(b) that when the separation distances between WECs increase, the interaction strength or oscillation amplitude decreases which implicitly means that available wave energy from ocean waves to capture decreases. This can be clearly observed in Figure 2(b) between sway IRFs of K_{12} and K_{13}.

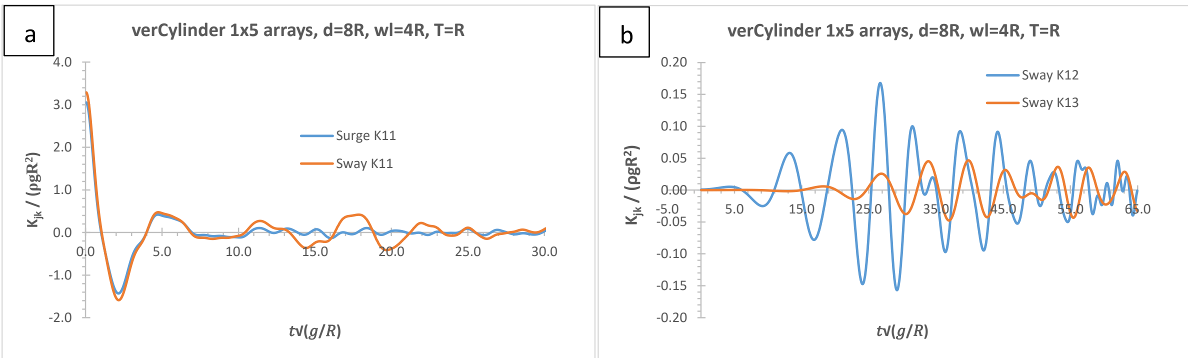

Figure 2: Linear 1x5 arrays of truncated vertical cylinder in front of a vertical wall with radius R, d=8R, wl=4R, draft T=R; (a) surge and sway diagonal IRFs of K_{11} for WEC1; (b) sway interaction IRFs of K_{12} and K_{13}.

Figure 3(a) and (b) show the dimensionless diagonal added-mass (A_{11}^{11}) and damping (B_{11}^{11}) coefficients in surge mode for 1x5 arrays of truncated vertical cylinder, respectively. The present ITU-WAVE numerical results are compared with analytical results of Konispoliatis et.al. (2020). The comparison of present numerical results with analytical results shows satisfactory agreements as can be seen in Figure 3(a) and (b). In the context of linear analysis, time and frequency domain results are dependent on each other through Fourier transform. The frequency dependent added-mass (A_{11}^{11}) in Figure 3(a) and damping (B_{11}^{11}) in Figure 3(b) coefficients are obtained by taking Fourier transform of time dependent diagonal surge IRFs (K_{11}) of Figure 2(a).

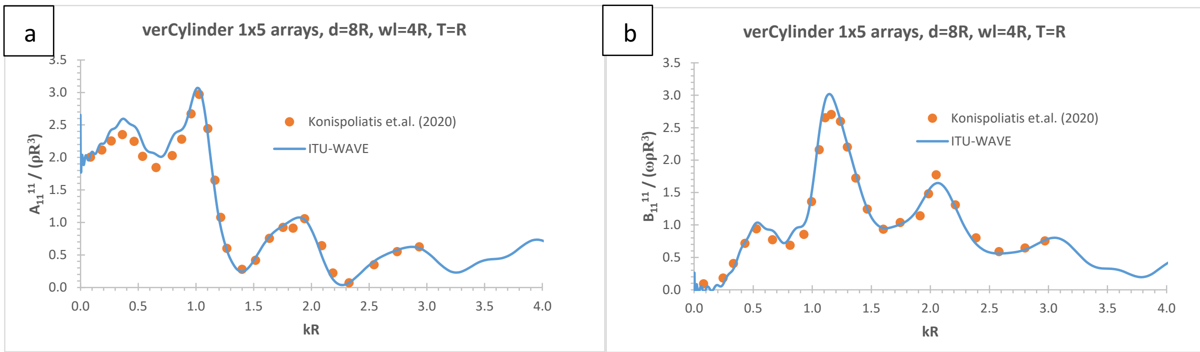

Figure 3: Surge dimensionless diagonal radiation force coefficients of WEC1; (a) A_{11}^{11}; (b) B_{11}^{11}.

Figure 4(a) and (b) show the dimensionless interaction added-mass (A_{22}^{12}) and damping (B_{22}^{12}) coefficients in sway mode between WEC1 and WEC2 for 1x5 arrays of truncated vertical cylinder. The present ITU-WAVE results are compared with analytical results (Konispoliatis et.al. 2020) which show satisfactory agreements.

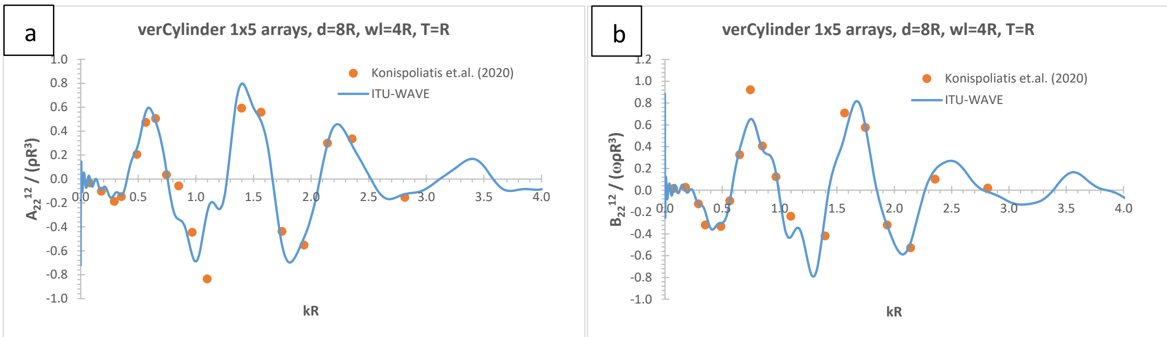

Figure 4: Sway dimensionless radiation interaction force coefficients between WEC1 and WEC2; (a) A_{22}^{12}; (b) B_{22}^{12}.

3.1.2. Truncated vertical cylinder of 2x2 arrays in front of a vertical wall – exciting forces

The nondimensional exciting IRFs (K_{2E}) in sway mode for 2x2 arrays of truncated vertical cylinder at incident wave angle of 270° are presented in Figure 5. The exciting IRFs for WEC1 and WEC2 as well as WEC3 and WEC4 are the same due to the symmetry of WECs with respect to the heading angle of 270°.

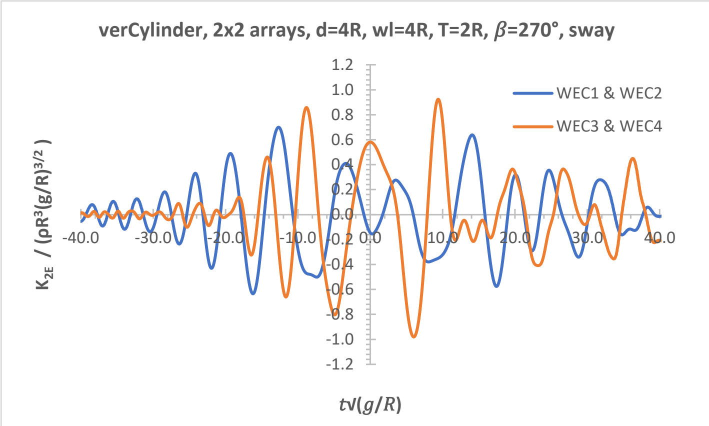

Figure 5: Sway nondimensional exciting force IRFs (K_{2E}) of square 2x2 arrays of truncated vertical cylinder in front of a vertical wall.

The dimensionless sway exciting force amplitudes of square 2x2 arrays of truncated vertical cylinders at the incident wave angle of 270° are compared with the numerical results of Chatjigeorgiou (2019) for WEC1 & WEC2 and WEC3 & WEC4 in Figure 6(a) and 6(b) respectively. The present frequency dependent sway exciting force amplitudes of ITU-WAVE numerical results and those of Chatjigeorgiou (2019) show satisfactory agreements. The wave exciting force amplitudes for WEC1 and WEC2 as well as WEC3 and WEC4 are obtained via Fourier transform of exciting IRFs of Figure 5 in sway mode. As in sway exciting IRFs of Figure 5, the exciting force amplitude of WEC1 and WEC2 as well as WEC3 and WEC4 are the same due to the symmetry of WECs with respect to incident wave angle of 270°.

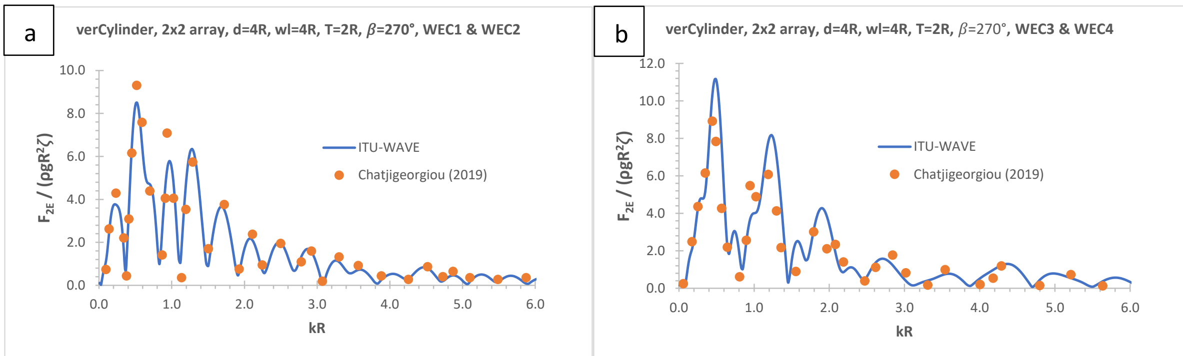

Figure 6: Sway nondimensional exciting force amplitudes (F_{2E}); (a) WEC1 and WEC2; (b) WEC3 and WEC4.

3.1.3. Vertical cylinder with hemisphere bottom of 2x5 arrays – mean interaction factor

The heave exciting force IRFs and amplitudes of 2x5 arrays of vertical cylinder with hemisphere bottom are presented in Figure 7(a) and 7(b) respectively. It may be noticed in Figure 7(a) and 7(b) that heave exciting IRFs and force amplitudes of WEC1, WEC2, WEC3, WEC4, WEC5 and WEC6, WEC7, WEC8, WEC9, WEC10 are the same due to the symmetry of WECs with respect to incident wave angle of 90°.

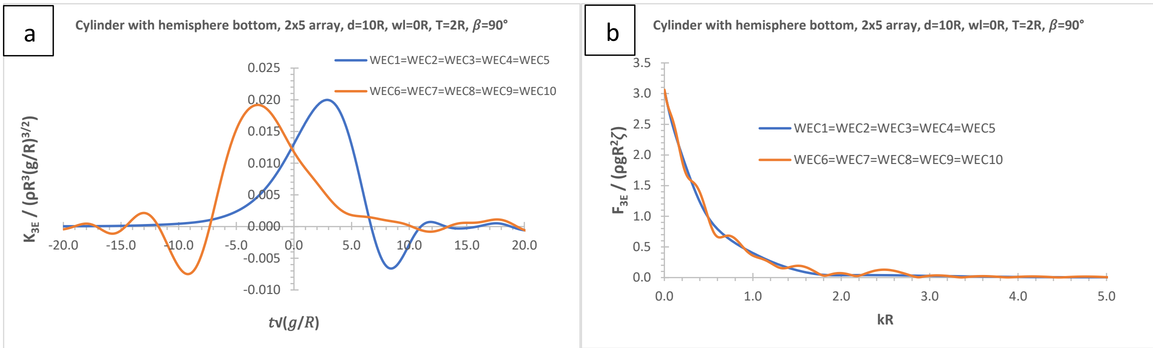

Figure 7: Heave dimensionless exciting force of rectangle 2x5 arrays of vertical cylinder with hemisphere bottom without wall effect; (a) K_{3E} ; (b) F_{3E}.

The dimensionless heave diagonal and interaction radiation IRFs are presented in Figure 8(a) and 8(b). When heave diagonal IRF (K_{11}) is compared with interaction K_{12}, K_{13}, K_{14} and K_{15} where K_{15} represents the interaction IRF between WEC1 and WEC5, it can be observed in Figure 8(a) that diagonal IRF (K_{11}) is almost 8 times greater than interaction IRFs. When the separation distances between WECs increase in Figure 8(b), the amplitudes of interaction IRFs decrease. This implicitly means that hydrodynamic interactions between WECs are weaker. The interaction IRFs decay to zero after a few oscillations in the case of closer proximity (e.g., K_{16}, K_{17}) in Figure 8(b) whilst, when the separation distance between WECs increases, it takes longer times for interaction IRFs to decay to zero and oscillations with greater amplitudes shift to longer times (e.g., K_{19}, K_{110}).

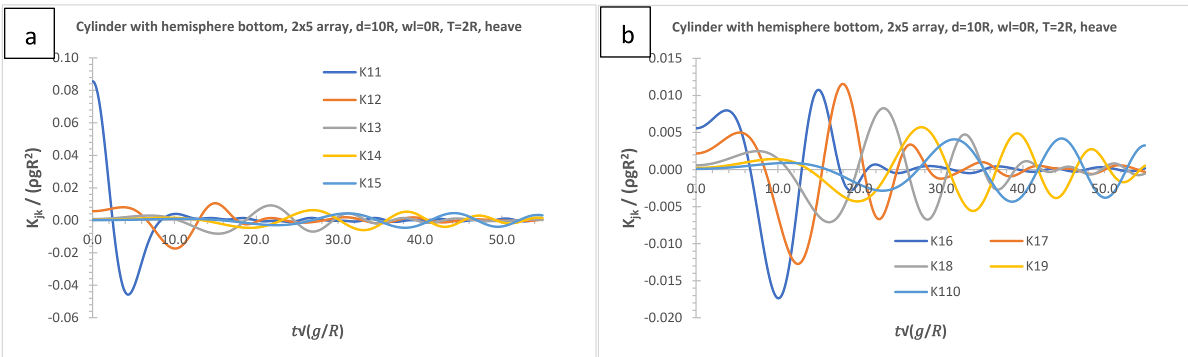

Figure 8: Heave dimensionless diagonal and interaction radiation force IRFs; (a) $K_{11} – K_{15}$; (b) $K_{16} – K_{110}$.

The dimensionless heave diagonal and interaction hydrodynamic coefficients are presented in Figure 9(a) and 9(b) for added-mass and in Figure 10(a) and 10(b) for damping coefficients. Figure 9(a) and 10(a) represent the diagonal and interaction added-mass and damping coefficients of 1st row of 2x5 arrays whilst 2nd row results are presented in Figure 9(b) and 10(b) respectively. When the separation distances increase between WECs, the amplitudes of interaction added-mass and damping coefficients decrease in Figure 9(b) and 10(b). It may be also noticed that when the separation distances increase between WECs, the interaction added-mass and damping coefficients require more oscillation to decay to zero.

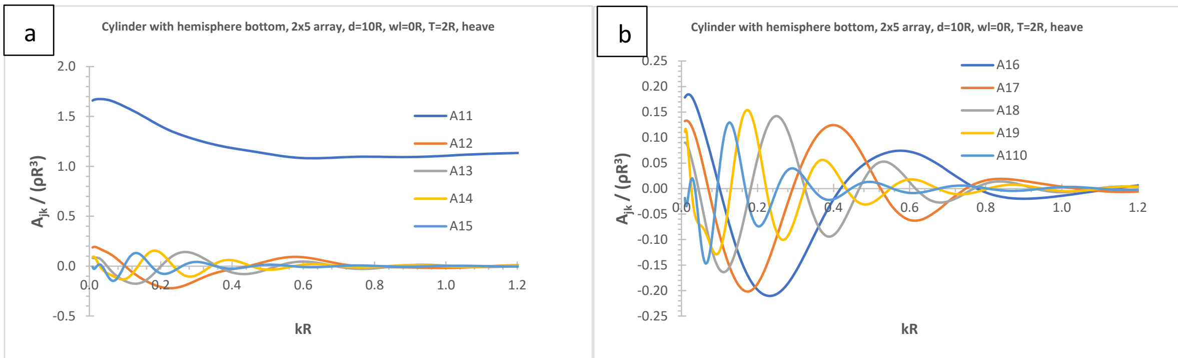

Figure 9: Heave dimensionless diagonal and interaction added-mass coefficients; (a) A_{11}- A_{15}; (b) A_{16}- A_{110}.

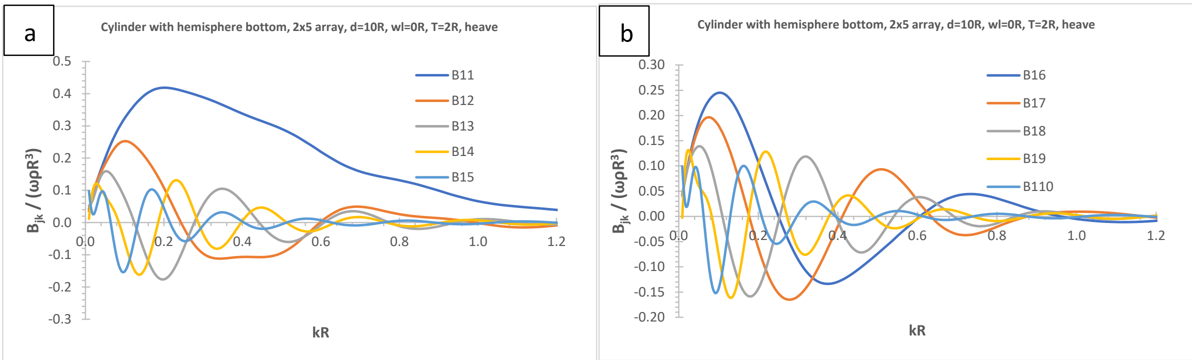

Figure 10: Heave dimensionless diagonal and interaction damping coefficients; (a) B_{11}- B_{15}; (b) B_{16}- B_{110}.

The predicted mean interaction factor of ITU-WAVE is compared with numerical result of McCallum et.al. (2014) in Figure 11. The present ITU-WAVE numerical result shows satisfactory agreement with that of McCallum et.al. (2014). In addition to mean interaction factor, which is the sum of mean interaction factor of 1st row (WEC1-WEC5) and 2nd (WEC6-WEC10) row of 2x5 arrays system, the mean interaction factors of 1st and 2nd rows are also presented in Figure 11. The mean interaction factor of 2nd row, which is in the wake of 1st row that meets with the incident wave first, is greater and has more constructive effect compared to 1st row. This is mainly due to the strong hydrodynamic interactions and nearly trapped waves in the gap of 1st and 2nd rows of WECs in an array system. The mean interaction factor has maximum constructive effect at dimensionless natural frequency of 0.5 whilst it has destructive effect at about dimensionless incident wave frequency of 0.6. The mean interaction factor oscillates about q_{mean} = 1.0 up to dimensionless incident wave frequency of 0.4 which means that the same amount of wave energy from ocean waves is absorbed with isolated WECs and rectangle 2x5 arrays whilst mean interaction factor has mainly constructive effects at dimensionless higher incident wave frequencies.

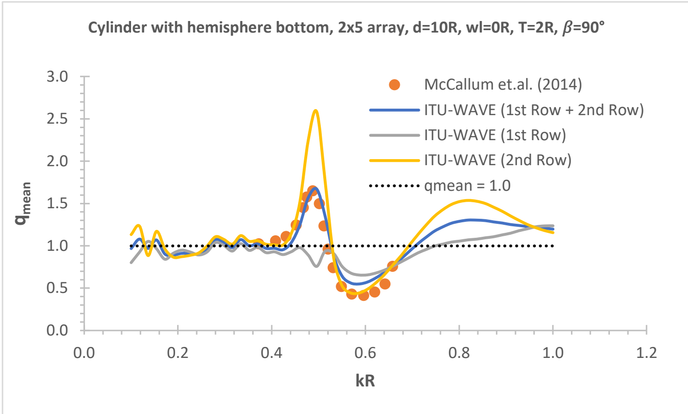

Figure 11: Mean interaction factor q_{mean} of rectangle 2x5 arrays of vertical cylinder with hemisphere bottom without a vertical wall effect.

3.2. Radiation and exciting force IRFs

The dimensionless exciting force IRFs of 1x5 arrays of sphere with radius R are presented in Figure 12. The IRFs for WEC1 and WEC5 as well as WEC2 and WEC4 are the same due to symmetry of WECs with respect to heading angle of 90^o for both with and without vertical wall effects. When with and without vertical wall effects are compared, the bandwidth of the IRFs with vertical wall effects are greater than that of without vertical wall effect. As the area under IRFs represents the available energy to be absorb with WECs, Figure 12 implicitly shows that more energy is available in the case of WECs arrays in front of a vertical wall due to wider bandwidths. The IRFs with vertical wall effects start to oscillate much earlier. This also implicitly means that WECs in an array system feel the effect of incident waves earlier in the case of WECs placed in front of a vertical wall.

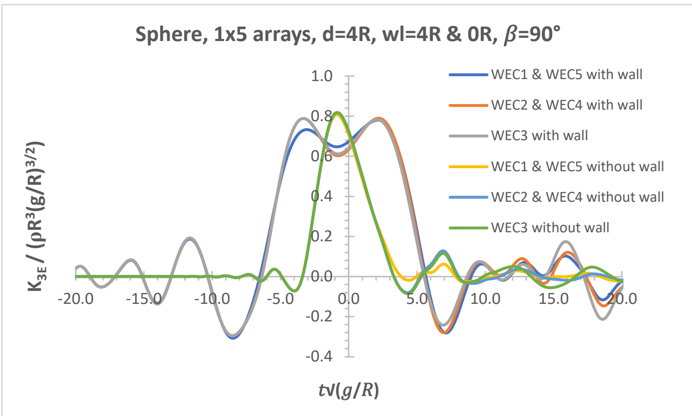

Figure 12: Heave dimensionless exciting force IRFs of 1x5 arrays of sphere with and without vertical wall effects.

The dimensionless heave exciting force IRFs at the middle of each row of 5x5 arrays of sphere without and with vertical wall effects are presented in Figure 13(a) and 13(b) respectively. Although the exciting force amplitudes of IRFs without and with vertical wall effects are approximately the same, the bandwidth of heave exciting force IRFs are greater in the case of WECs arrays in front of a vertical wall. This implicitly means that as mentioned before, more wave energy from ocean waves would be absorbed with WECs arrays placed in front of a vertical wall.

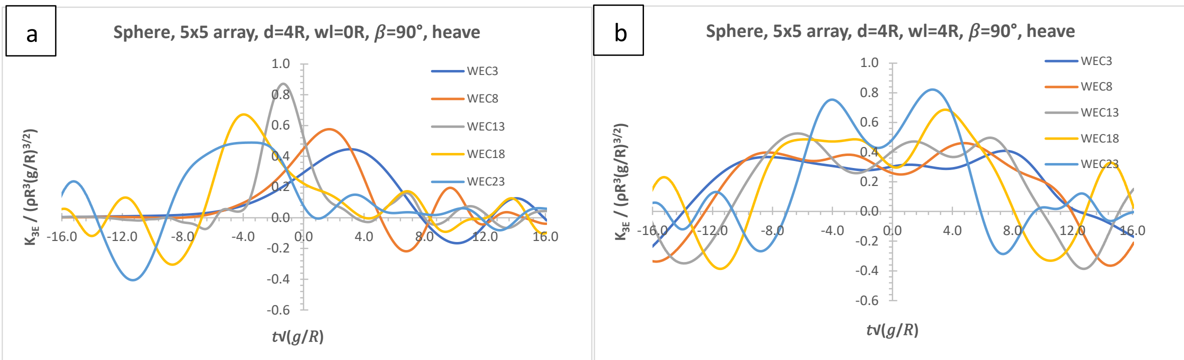

Figure 13: Heave dimensionless exciting force IRFs at the middle of each row of 5x5 arrays of sphere; (a) without vertical wall effect; (b) with vertical wall effect.

The dimensionless heave radiation interaction IRFs of 1x5 arrays of sphere without and with vertical wall effects are presented in Figure 14(a) and 14(b) respectively. When radiation force IRFs with and without vertical wall effects are compared, the amplitude of IRFs with vertical wall effects are greater compared to those of without vertical wall effects at longer times although the amplitudes of interaction IRFs are approximately the same at lower times. As in the case of exciting IRFs, the greater amplitude of interaction radiation IRFs at larger times implicitly means that the more wave energy is available to be absorb. It may be also noticed that the interaction effects are greater at closer proximity of WECs whilst the greater interaction effects are shifted to longer times when the separation distances between WECs are increased.

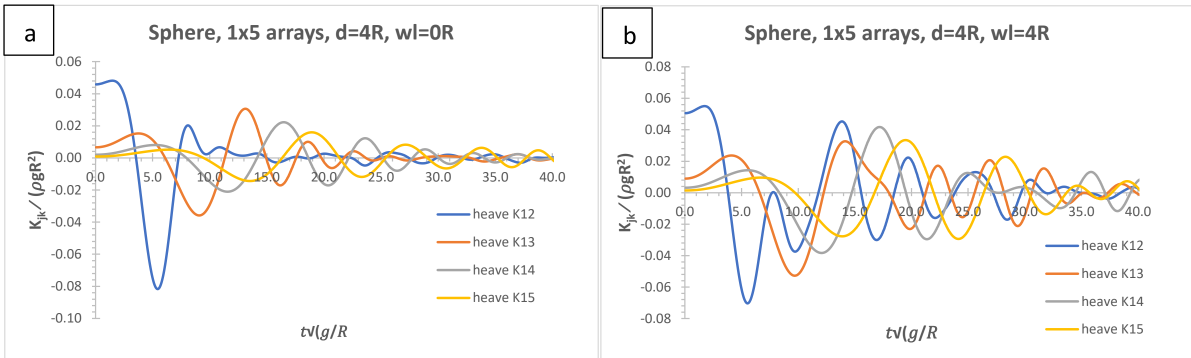

Figure 14: Heave dimensionless radiation interaction IRFs of 1x5 arrays of sphere; (a) without vertical wall effect; (b) with vertical wall effect.

3.3. Response Amplitude Operators (RAOs) of WECs in an array system

The sway and heave RAOs with 1x5 arrays of sphere in front of a vertical wall at heading angles 90° are presented in Figure 15(a) and 15(b) respectively. The RAOs for WEC1 and WEC5 as well as WEC2 and WEC4 in Figure 15(a) and 15(b) are the same due to the symmetry of WECs with respect to incident wave angle 90°. It may be also noticed that there are three resonance occourences in both sway and heave modes, but magnitude of the resonances are finite.

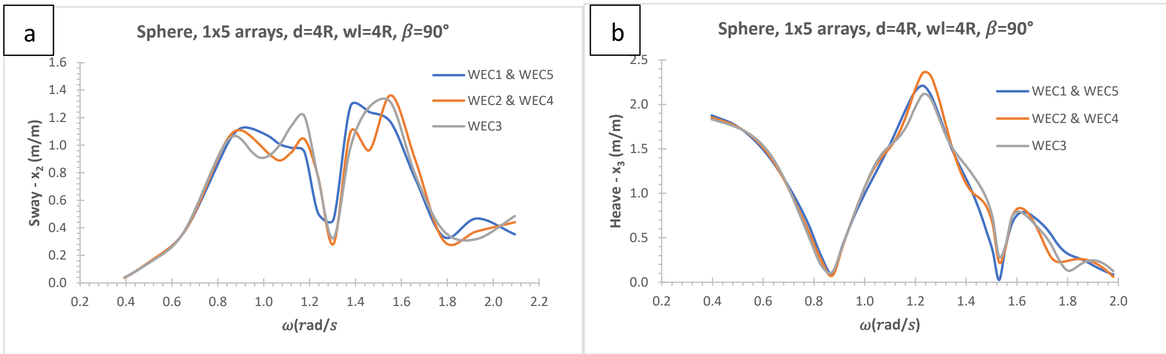

Figure 15: RAOs for each WEC in 1x5 arrays of sphere in front of a vertical wall; (a) sway; (b) heave.

The RAOs for sway and heave modes with 2x5 arrays in front of a vertical wall at heading angle 90° are presented in Figure 16(a), 16(b), 16(c) and 16(d) for 1st and 2nd rows of sway mode as well as 1st and 2nd rows of heave mode respectively. The incident wave meets 1st row WECs first and 2nd row WECs are located at the wake of 1st row. There are three sway and six heave resonance occourances for 1st row WECs. These resonances are finite which means that some of the wave energy are radiated back to sea due to oscillations of WECs in an array system. These resonance occurrences in sway and heave modes are due to hydrodynamic interaction in the wave motion between WECs as well as WECs and a vertical wall when the WECs in the array system are forced to oscillate on the free surface. The motions of the fluid between WECs as well as WECs and a vertical wall are strongly excited at frequencies corresponding to standing waves. An occurrence of complete reflection or complete transmission of incident waves is possible at standing wave frequencies where wave motion between WECs as well as WECs and a vertical wall is resonant (Newman, 1974; Evans, 1975). The sway and heave RAOs for 2nd row WECs are greater than those of 1st row due to the standing and nearly trapped waves between gaps of WECs in an array system as well as WECs and a vertical wall. Both sway and heave RAOs of WEC1 and WEC5 as well as WEC2 and WEC4, which are the 1st row WECs in 2x5 rectangular arrays, are the same due to symmetry of WECs with respect to incident wave at heading angle 90° in Figure 16(a) and (c). It is also true that the RAOs of WEC6 and WEC10 as well as WEC7 and WEC9 in both sway and heave modes, which are the 2nd row WECs, are the same due to symmetry of WECs with respect to incident wave angle of 90° in Figure 16(b) and (d).

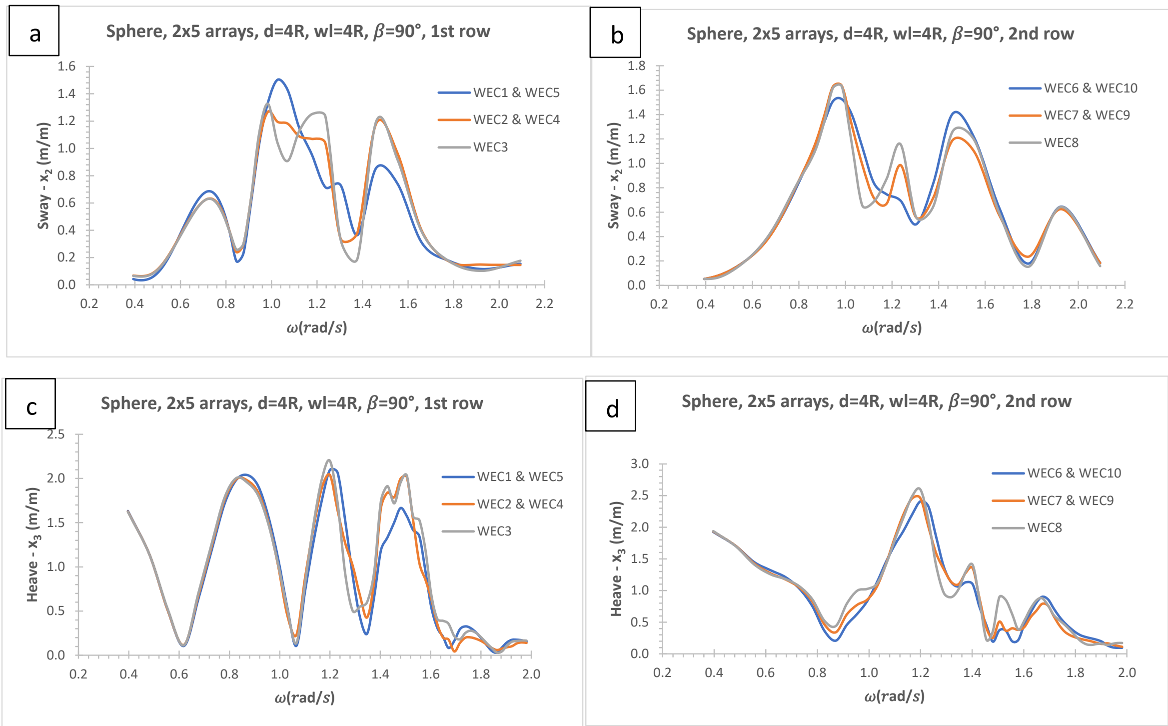

Figure 16: RAOs for each WEC in 2x5 arrays of sphere in front of a vertical wall; (a) sway – 1st row; (b) sway – 2nd row; (c) heave – 1st row; (d) heave – 2nd row.

3.4. Absorbed wave power with isolated, 1x5 and 2x5 arrays in front of a vertical wall

The sway and heave RAOs and absorbed wave power with an isolated sphere at heading angle 90° are presented in Figure 17(a) and 17(b) respectively. As floating systems (e.g., sphere WEC) do not have the restoring force at sway mode, it is assumed in the present study that PTO restoring force coefficients at sway and heave modes are equal. This means both sway and heave modes have the same displacements which implies that the performances of sphere at both modes can be directly compared against each other. As it may be observed in Figure 17(b) and is theoretically known (Budal and Falnes 1976) that the maximum wave power is captured at resonant frequency at which natural frequency of sphere (w=1.38 rad/s) at both sway and heave modes are equal to incident wave frequency. It may be noticed in Figure 17(b) that more wave power is absorbed at resonant frequency at sway mode than heave mode. The absorption bandwidth in Figure 17(b) is much wider at sway mode at higher frequencies although heave mode absorbs more power at lower frequencies at which more wave energy is available to be absorb.

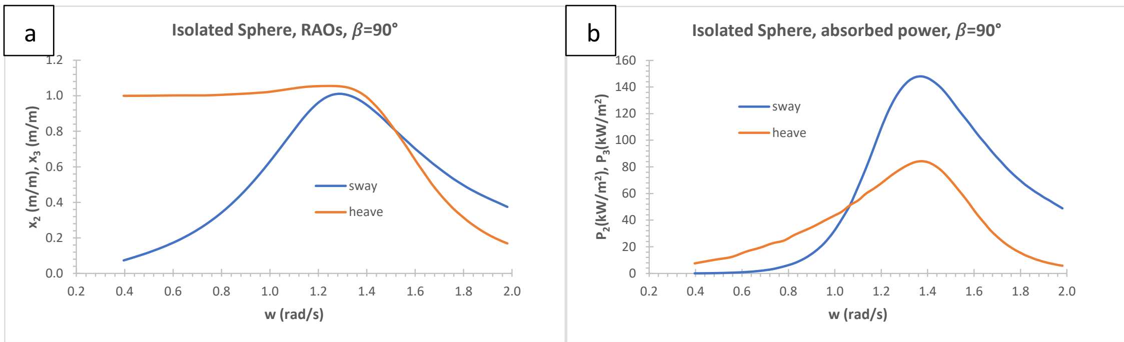

Figure 17: Isolated sphere with radius R in sway and heave modes; (a) RAOs; (b) absorbed power.

The absorbed wave power with 1st row, 2nd row and superpositions of 1st and 2nd rows using 2x5 arrays of sphere in front of a vertical wall at heading angles 90° is presented in Figure 18(a) and 18(b) for sway and heave modes respectively. The wave energy absorbtion in heave mode in Figure 18(b) is concentrated at wave frequencies of 1.2 and 1.5 rad/s whilst it is distributed in a range of incident wave frequencies with much wider frequency bandwidth in sway mode in Figure 18(a). The absorption with sway mode in Figure 18(a) are greater at around incident wave frequency of 1.0 and 1.5 rad/s. More wave power is absorbed in sway mode in Figure 18(a) with 2nd row WECs, which are at the wake of 1st row. The maximum wave power in Figure 19(b) is absorbed at the same incident wave frequency of 1.2 rad/s with 1st and 2nd row WECs with heave mode although 2nd row WECs absorb much greater wave power at incident wave frequency of 1.5 rad/s.

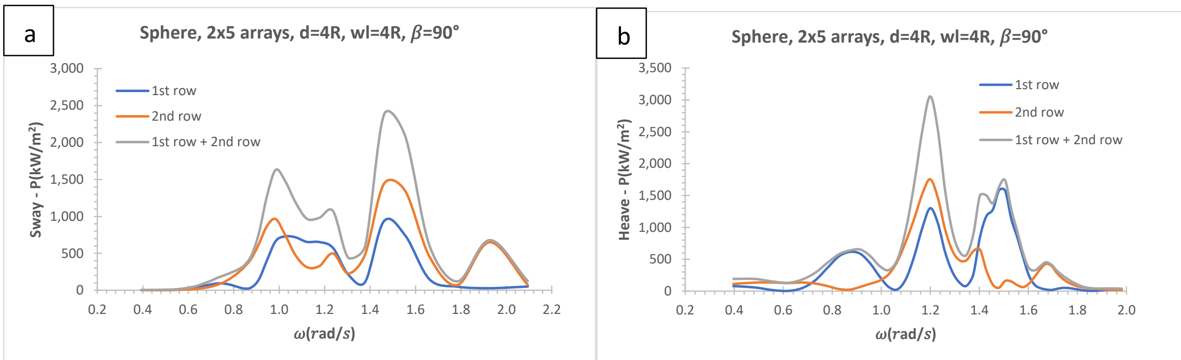

Figure 18: Absorbed wave power with 2x5 arrays of sphere in front of a vertical wall; (a) sway (b) heave mode.

When the absorbed wave power with isolated WEC in Figure 17(b) and 2x5 WEC arrays in Figure 18(a) and (b) are compared, it may be noticed that much more power is absorbed in sway mode with isolated WEC at around natural frequency region. However, in the case of 2x5 arrays, the absorbed power in sway and heave modes are comparable in Figure 18(a) and 18(b). The maximum wave power is absorbed in heave mode at around 1.2 rad/s compared to sway mode in a range of incident waves.

3.5. Mean interaction factors of 3x5 and 5x5 arrays of sphere without a vertical wall effect

Mean interaction factors q_{mean} of each row of sphere with 3x5 and 5x5 arrays are presented in Figure 19(a) and 19(b) respectively. It can be observed that higher row numbers (e.g., 3rd row for 3x5 arrays and 4th and 5th rows for 5x5 arrays) has better constructive effects compared to lower row numbers especially at higher incident wave frequencies (e.g., 1st row) which meet with incident wave first. When the row numbers increase, the destructive effect of lower row numbers increases (e.g., 1st and 2nd rows). This may be noticed when mean interaction factor of 1st rows in Figure 19(a) and 19(b) are compared.

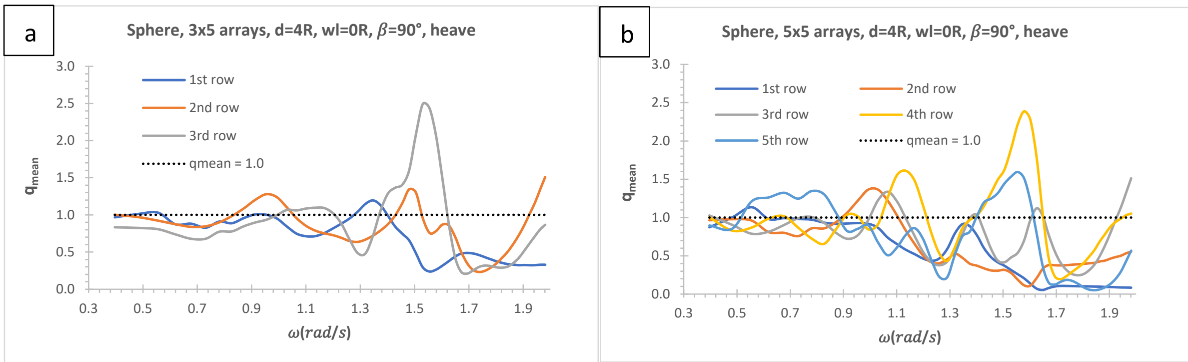

Figure 19: Mean interaction factors of sphere without vertical wall effect in heave mode; (a) 3x5 arrays; (b) 5x5 arrays.

3.5.1. Mean interaction factors of sphere with 3x5 and 5x5 arrays in front of a vertical wall

Mean interaction factors q_{mean} of sphere with 3x5 and 5x5 arrays in front of a vertical wall in heave mode are presented for each row in Figure 20(a) and 20(b) respectively. It may be noticed that when the rows are closer to vertical wall, mean interaction factors are greater compared to the rows which are away from a vertical wall (e.g., 3rd and 2nd rows for 3x5 sphere arrays whilst 5th and 4th rows for 5x5 arrays). When the row numbers increase in an array system, the contributions of the rows away from a vertical wall to wave absorption in Figure 20(b) are mostly destructive (e.g., 1st, 2nd, and 3rd rows at especially higher frequencies).

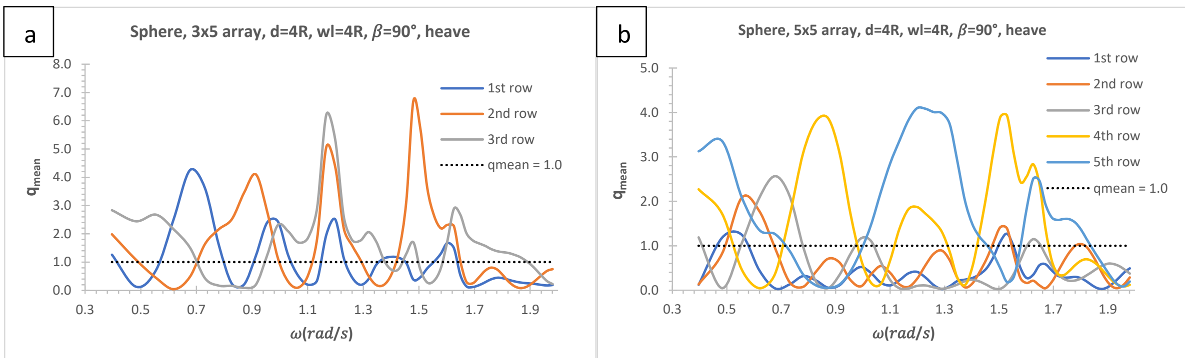

Figure 20: Mean interaction factors of each row of sphere in front of a vertical wall in heave mode; (a) 3x5 arrays; (b) 5x5 arrays.

3.5.2. Mean interaction factors of sphere in a range of arrays with and without a vertical wall effect

Mean interaction factors without and with a vertical wall effect for sphere WECs of 1x5, 2x5, 3x5, 4x5 and 5x5 arrays in heave mode in a range of incident wave frequencies are presented in Figure 21(a) and 21(b) respectively. In the case of 1x5 arrays of sphere in front of a vertical wall, the behaviour of mean interaction factors shows constructive effect apart from about incident wave frequencies of 0.87 and 1.53 rad/s. When other array configurations in front of a vertical wall are considered, mean interaction factors of 2x5, 3x5, 4x5 and 5x5 arrays have the constructive effects in a range of the incident wave frequency up to 1.7 rad/s, however, after this incident wave frequency, mean interaction factors show destructive effects. The magnitudes of the constructive effects decrease with increasing row numbers at lower incident wave frequencies in Figure 21(b). Mean interaction factors of 2x5, 3x5, and 4x5 arrays in Figure 21(b) also show 2.2 times constructive effects up to incident wave frequency of 1.1 rad/s whilst the constructive effects of 1x5, 2x5, and 3x5 arrays reach up to 4.65 times at incident wave frequency of 1.2 rad/s. However, these constructive effects decrease up to 2.3 and 1.4 for 4x5 and 5x5 arrays at the same incident wave frequency of 1.2 rad/s respectively. In the case of arrays without a vertical wall effect, the dominant incident wave frequency is around 1.5 rad/s for constructive effect whilst it is around 1.75 rad/s for destructive effect. When with and without a vertical wall effect are compared, it can be clearly observed from Figure 21(a) and (b) that the magnitudes of the constructive effects of WECs arrays in front of a vertical wall in Figure 21(b) are much greater almost all range of incident wave frequencies compared to without a vertical wall effect in Figure 21(a).

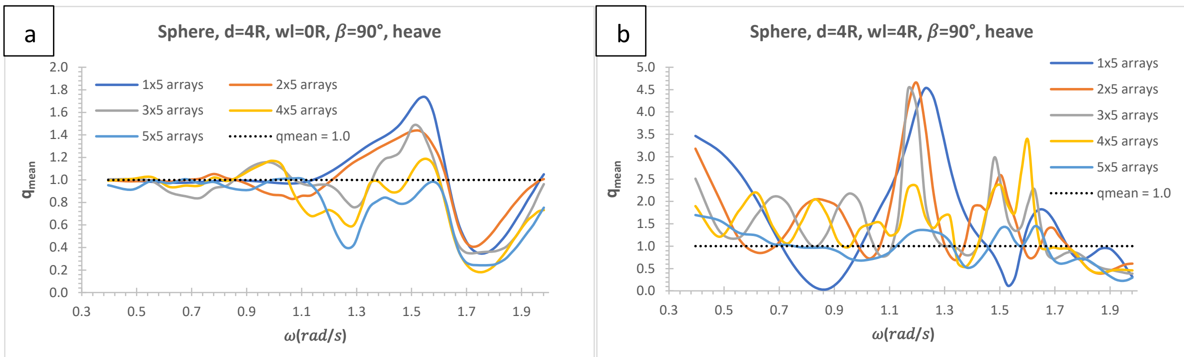

Figure 21: Mean interaction factors of sphere in heave mode in a range of row numbers and 5 column numbers; (a) without a vertical wall effect; (b) with a vertical wall effect.

4. Conclusions

The exploitation of the wave power absorption from ocean waves using WECs arrays with and without a vertical wall effect is analysed with in-house transient wave-multibody interaction computational tool of ITU-WAVE. The time dependent boundary integral equation method is used to solve the initial boundary value problem with time marching scheme whilst the perfect reflection of the incident waves from a vertical wall is predicted with method of images in ITU-WAVE numerical tool.

The amplitudes of the diagonal and interaction radiation IRFs are comparable at closer proximity. This implicitly means that WECs in an array system have strong hydrodynamic interactions due to standing waves and nearly trapped waves in the gap of WECs and a vertical wall. The numerical experiences also show that when the separation distances between WECs as well as WECs and a vertical wall increase, the interaction effects are getting weaker which means available wave energy to absorb from ocean waves decreases. In the case of wave exciting forces, exciting force IRFs with and without vertical wall effects are compared, it is observed that the bandwidth of exciting force IRFs with a vertical wall effect are greater which means that the available energy to absorb are also greater.

The nearly trapped and standing waves in the gap of WECs as well as WECs and a vertical wall in an array system play significant role for the maximum wave power absorption especially closer separation distances. It is found out by the numerical experiences that the mean interaction factors for all considered array systems are at least 2 times greater in the case of arrays in front of a vertical wall compared to arrays without a vertical wall effect. The constructive effect is also much greater than destructive effect in an array system in front of a vertical wall for all considered array systems.

Acknowledgements

The financial support of present work under UK-China Industry Academy Partnership Programme with contract number of Grant No: UK-CIAPP\73 by Royal Academy of Engineering Newton Fund is acknowledged.

References

Budal K. Theory for absorption of wave power by a system of interacting bodies. Journal of Ship Research, 1977, 21(4), 248-253.

Budal K, Falnes J. Optimum operation of wave power converter. Internal Report, Norwegian University of Science and Technology 1976.

Buriani F, Renzi E. Hydrodynamics of a flexible piezoelectric wave energy harvester moored a breakwater. European Wave and Tidal Energy Conference (EWTEC), 2017.

Chang MS. Computation of Three-Dimensional Ship Motions with Forward Speed. Proceedings of the 2nd International Symposium on Numerical Ship Hydrodynamics, University of California, Berkeley, 1977, 124-135.

Chatjigeorgiou IK. Semi-analytical solution for the water wave diffraction by arrays of truncated circular cylinders in front of a vertical wall. Applied Ocean Research, 2019, 88, 147-159.

Contestabile P, Di Lauro E, Buccino M, Vicinanza D. Economic assessment of overtopping breakwater for energy conversion (OBREC): a case study in western Australia. Sustainability, 2016, 9(1), 51.

Cummins WE. The Impulse response function and ship motions. Shiffstechnik, 1962, 9, 101-109.

Evans DV. A note on the total reflection or transmission of surface waves in the presence of parallel obstacles. Journal of Fluid Mechanics, 1975, 67, 465–472.

He F, Huang ZH, Law AWK. An experimental study of a floating breakwater with asymmetric pneumatic chambers for wave energy extraction. Applied Energy, 2013, 106, 222-231.

Hess JL, Smith AMO. Calculation of non-lifting potential flow about arbitrary three-dimensional bodies. Journal of Ship Research 1964, 8, 22-44.

Kagemoto H, Yue DKP. Interactions among multiple three-dimensional bodies in water waves: an exact algebraic method. Journal of Fluid Mechanics, 1986, 166, 189-209.

Kara F. Application of time domain methods for marine hydrodynamic and hydroelasticity analyses of floating systems. Ships and Offshore Structures, 2021.

Kara F. Multibody interactions of floating bodies with time domain predictions. Journal of Waterway, Port, Coastal, and Ocean Engineering, 2020, 146(5).

Kara F. Time domain prediction of power absorption from ocean waves with wave energy converters arrays. Renewable Energy, 2016a, 92, 30-46.

Kara F. Time domain prediction of seakeeping behaviour of catamarans. International Shipbuilding Progress, 2016b, 62(3-4).

Kara F. Time domain prediction of hydroelasticity of floating bodies. Applied Ocean Research, 2015, 51, 1-13.

Kara F. Time domain prediction of power absorption from ocean waves with latching control. Renewable Energy, 2010, 35, 423-434.

Kara F. Time domain hydrodynamics and hydroelastics analysis of floating bodies with forward speed. PhD thesis, University of Strathclyde, Glasgow, UK 2000.

King BW. Time domain analysis of wave exciting forces on ships and bodies. PhD thesis*,* The University of Michigan, Ann Arbor, Michigan, USA, 1987.

Konispoliatis DN, Mavrakos SA and Katsaounis GM. Theoretical evaluation of the hydrodynamic characteristics of arrays of vertical axisymmetric floaters of arbitrary shape in front of a vertical breakwater. Journal of Marine Science and Engineering, 2020, 8, 62.

Kring DC, Sclavounos PD. Numerical stability analysis for time-domain ship motion simulations Journal of Ship Research, 1995, 39 (4), 313-320.

Liapis S. Time Domain Analysis of Ship Motions. PhD thesis, The University of Michigan, Ann Arbor, Michigan, USA 1986.

Loukogeorgaki E, Boufidi I, Chatjigeorgiou IK. Performance of an array of oblate spheroidal heaving wave energy converters in front of a wall. Water, 2020, 12, 188.

McCallum P, Venugopal V, Forehand D, Sykes R. On the performance of an array of floating wave energy converters for different water depths. Proceedings of the ASME, 33^{rd} International Conference on Ocean, Offshore and Arctic Engineering, 2014, OMEA2014, June 8-13, USA.

McIver P, Porter R. The motion of a freely floating cylinder in the presence of a wall and the approximation of resonances. Journal of Fluid Mechanics, 2016, 795, 581–610.

Michele S, Renzi E, Sammarco P. Weakly nonlinear theory for a gate-type curved array in waves. Journal of Fluid Mechanics, 2019, 869, 238-263.

Michele S, Sammarco P, d'Errico M. The optimal design of a flap gate array in front of a straight vertical wall: Resonance of the natural modes and enhancement of the exciting torque. Ocean Engineering, 2016, 118, 152-164.

Mustapa MA, Yaakob OB, Ahmed YM, Rheem C.-K, Koh KK, Adnan FA. Wave energy device and breakwater integration: A review. Renewable and Sustainable Energy Reviews, 2017, 77, 43–58.

Nakos D, Kring D, Sclavounos PD. Rankine Panel Method for Transient Free Surface Flows. Proceedings of the 6^{th} International Symposium on Numerical Hydrodynamics, Iowa City, I.A., USA, 1993, 613-632.

Newman JN. Interactions of water waves with two closely spaced vertical obstacles. Journal of Fluid Mechanics, 1974, 66, 97–106.

Newman JN. Channel wall effects in radiation-diffraction analysis, 31^{st} International Workshop on Water Waves and Floating Bodies, 2016.

Ning DZ, Zhao XL, Goteman M, Kang HG. Hydrodynamic performance of a pile-restrained WEC-type floating breakwater: an experimental study. Renew Energy, 2016, 95, 531-541.

Ogilvie TF. Recent progress toward the understanding and prediction of ship motions. Proceedings of the 5^{th} Symposium on Naval Hydrodynamics, Office of Naval Research, Washington, D.C., USA, 1964, 3-128.

Ohkusu M. Wave action on groups of vertical circular cylinders. Journal of the Society of Naval Architects in Japan, 1972, 131.

Sarkar D, Renzi E, Dias F. Effect of a straight coast on the hydrodynamics and performance of the Oscillating Wave Surge Converter. Ocean Engineering, 2015, 105, 25-32.

Schay J, Bhattacharjee J, Soares CG. Numerical Modelling of a Heaving Point Absorber in front of a Vertical Wall. In Proceedings of the ASME 32nd International Conference on Ocean, Offshore and Arctic Engineering, Nantes, France, 9–14 June 2013.

Thomas GP, Evans DV. Arrays of three-dimensional wave-energy absorbers. Journal of Fluid Mechanics, 1981, 108, 67-88.

Wehausen JV, Laitone EV. Surface Waves in Fluid Dynamics III in Handbuch der Physik 1960; Chapter 3:446-778

Zhao XL, Ning DZ, Zou QP, Qiao DS, Cai SQ. Hybrid floating breakwater-WEC system: A review. Ocean Engineering, 2019a, 186, 106-126.

Zhao XL, Ning DZ, Liang DF. Experimental investigation on hydrodynamic performance of a breakwater integrated WEC system. Ocean Engineering, 2019b, 171, 25-32.

Zheng S, Zhang Y.Wave radiation from a truncated cylinder in front of a vertical wall. Ocean Engineering, 2016, 111, 602–614.